Model-Based Evaluation of Control Roll, Pitch and Yaw Moments for a Robotic Hummingbird

Siemen Timmermans [a], Frederik Leys [b], and Dirk Vandepitte [c]
KU Leuven, Celestijnenlaan 300, Box 2420, Leuven 3001, Belgium.

I. Introduction

Nano air vehicles with a span of around 15 cm have a size that is similar to small birds and insects. These animals generate thrust, which is defined as a vertical force, by flapping their wings. Produced thrust exceeds the values calculated with classical aerodynamics [1]. This observation implies advantages in terms of manoeuvrability and energy consumption. The implementation in a flying nanorobot requires the comparison to both fixed and rotary wings, based on an objective quantification of manoeuvrability. Thorough understanding of the mechanisms of thrust and drag generation is necessary.

Many authors use a computational fluid dynamics (CFD) model [2–9]. Solution of the Navier-Stokes equations provides instantaneous thrust and drag forces. The major disadvantage is a high computational load.

This paper uses a complete quasi-steady model for the calculation of the forces generated by the flapping wings [10–15]. Such a model is sufficiently accurate and much less demanding in terms of computational power. Force components are estimated based on the instantaneous horizontal and rotational velocity of the wing in a procedure similar to Karasek and Preumont [13] or Anderson and Cobb [15].

In addition to thrust, prescribed unsymmetrical motion of both wings generates steering moments. Several methods to generate moments are proposed in literature [12, 16–20]. The current study quantifies and compares the moments which are generated. Numerical values are computed

[a] Ph.D. Researcher, Department of Mechanical Engineering, siemen.timmermans@kuleuven.be
[b] Ph.D. Researcher, Department of Mechanical Engineering
[c] Professor, Department of Mechanical Engineering, Senior Member AIAA

for the specific case of the Kulibrie flapping wing nano air vehicle prototype, under certain assumptions which are specified in subsection II A. Comparison of results on the same model is objective and it supports the decision about the most effective methods to control the nanorobot.

II. Materials and methods

The Kulibrie nanorobot [21] is used as a reference flight vehicle. It is designed and built at KU Leuven. Several prototypes are available and design parameters can be changed relatively easily for experimental validation.

A. Wing and body

Fig. 1 shows the wing. R is the wing length, $c(r)$ is the chord length expressed as a function of distance from the wing root along the spar with a mean value $\bar{c}$, $\hat{r}_2$ is the dimensionless radius of second moment of wing area, S is the area of the wing surface, and $\hat{x}_0$ is the non-dimensional location of the wing hinge. Wing parameter values are listed in Table 1. The wing is considered to be a rigid flat plate. Most authors adopt the assumption of a flat plate, although verification of the validity of this assumption has not yet been provided. The resulting force generated by the wing acts at the centre of pressure, which is located at a distance $\hat{r}_2 \cdot R$ from the root of the wing and at a quarter of the chord length measured from the leading edge [13].

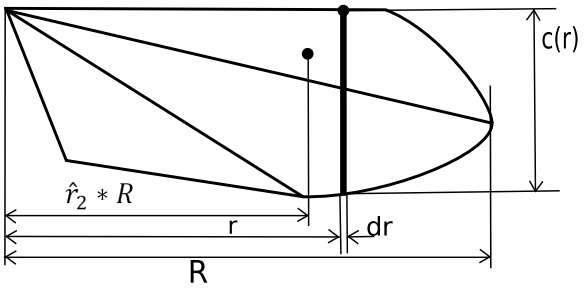

Fig. 1 Wing of the Kulibrie with wing parameters.

Table 1 Numerical values for the geometrical wing parameters of the Kulibrie.

R	$\bar{c}$	S	$\hat{r}_2$	$\hat{x}_0$
[mm]	[mm]	[mm^2]	[−]	[−]
67.2	20.8	1400	0.565	0

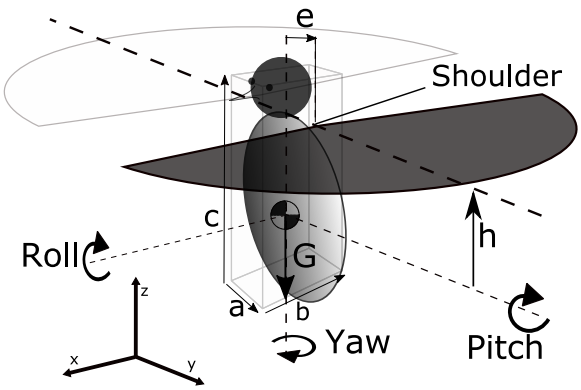

Fig. 2 Representation of the nanorobot with geometrical parameters.

Table 2 Numerical values for the geometrical body parameters of the Kulibrie.

a	b	c	G	I_{xx}	I_{yy}	I_{zz}	e	h
[mm]	[mm]	[mm]	[g]	[kgm^2]	[kgm^2]	[kgm^2]	[mm]	[mm]
20	25	60	14.5	$48.3 \cdot 10^{-5}$	$51 cdot 10^{-5}$	$12.4 \cdot 10^{-5}$	13	15

The body of the nanorobot is modelled as a beam element [18] with dimensions $a \times b \times c$ and a mass G (see Fig. 2). Mass is distributed symmetrically and centre of gravity is located in the plane of symmetry. The cuboid body is symmetrical and the only non-zero moments of inertia are I_{xx}, I_{yy}, I_{zz}. The root of the wing is called the shoulder and is shifted outward over a distance e. This shoulder joint can be shifted up and down and the vertical distance to the centre of gravity is h. Kulibrie parameter values are listed in Table 2. Aerodynamic interaction between the wing and the body is assumed to be negligible [7]. The thrust generated by the body and the drag on the body are not taken into account. The reference frame has the x-axis parallel to the longitudinal body axis and pointing forward, the y-axis parallel to the transversal body axis and pointing to the left, and the z-axis vertical and pointing upwards. This frame is used throughout the entire study in the different views of the nanorobot.

B. Wing kinematics

The primary flapping motion of the wing consists of two main components: a horizontal motion called the stroke motion and a rotary motion of the wing around the leading edge called the wing pitch. In this paper, the stroke motion takes place in the horizontal plane.

The stroke angle ϕ defines the stroke motion as a function of time [13]

$$\phi(t) = \phi_0 + \phi_{\mathrm{MAX}} \cos(2\pi f t) \tag{1}$$

where f is the flapping frequency [Hz], ϕ_0 is the mean wing stroke angle, ϕ_{MAX} is the stroke amplitude (see Fig. 3a). The mean wing stroke angle ϕ_0 is the angle at mid-stroke. Typical Kulibrie parameter values are listed in Table 3.

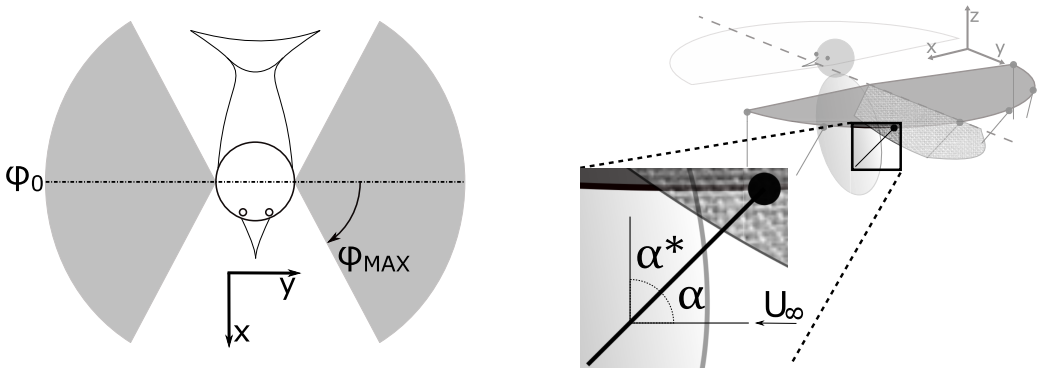

a) b)

Fig. 3 Geometrical wing parameters: a) top view of the Kulibrie with parameters of the stroke motion and b) inclination angle α and complementary angle α^*.

Wing pitch is described by the inclination angle α. In the formulas the complementary angle $\alpha^* = 90° - \alpha$ is also used (see Fig. 3b). The analytical formula for α^* as a function of time [13] is

$$\alpha^* = \begin{cases} \left(\frac{\pi}{2} - \alpha_m\right) + \frac{\pi - 2\alpha_m}{\Delta t_r}\left(t - t_0 - \frac{\Delta t_r}{2\pi}\sin\left(\frac{2\pi(t-t_0)}{\Delta t_r}\right)\right) & \text{for } t_0 \le t < t_1 \\ \frac{\pi}{2} - \alpha_m & \text{for } t_1 \le t < t_2 \\ \vdots & \vdots \end{cases} \tag{2}$$

where α_m is the value of α at mid-stroke, Δt_r is the total duration of wing pitch, $\{t_0,\ t_1,\ t_2, ...\}$ are time constants. The total duration of the wing pitch is expressed as a percentage of the total stroke duration. Typical Kulibrie parameter values are listed in Table 3.

The timing of the wing pitch phase with respect to wing stroke phase has an important influence on the force generation. The wing pitch phase can be advanced, delayed or symmetrical with respect to the wing stroke phase [5, 7]. To take the effect of the timing into account, a parameter ψ is added in the analytical expressions. A positive value for ψ refers to advanced rotation and a negative value

to delayed rotation. ψ is expressed as a fraction of a full flapping cycle. A typical value for ψ is shown in Table 3.

Table 3 The wing motion parameters and values in the reference flight set-up.

f	ϕ_{MAX}	ϕ_0	α_m	Δt_r	ψ
[Hz]	[°]	[°]	[°]	[%]	[%]
25	80	0	45	23	4.5

The wing motion parameters directly affect the velocity profile of the wing and, as a result, the thrust and drag generation. Wing motion parameters used in the next sections are summarized in Table 3.

C. Mathematical model

A quasi-steady model [11–13] is used for the calculation of aerodynamic forces. The model is designed to closely approximate the real aerodynamic thrust and drag forces. Instantaneous thrust and drag are assumed to depend solely on the velocity and the inclination of the wing at a given instant of time. Wing motion is prescribed by the analytical expressions for stroke (1) and wing pitch (2).

Trust and drag forces are calculated from the wing kinematics. Fig. 4 defines the force components which are used in the following sections.

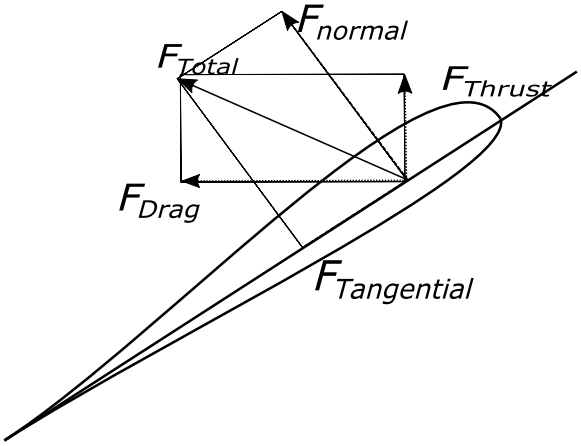

Fig. 4 Definition of the different force directions.

a. Stroke motion

Calculation of thrust and drag during the stroke motion is based on *thin airfoil theory* [22]. Normal and tangential force components are expressed as, respectively

$$F_N = \frac{1}{2}\rho C_N(\alpha) S \hat{r}_2^2 R^2 \dot{\phi}^2 \tag{3}$$

$$F_T = \frac{1}{2}\rho C_T(\alpha) S \hat{r}_2^2 R^2 \dot{\phi}^2 \tag{4}$$

where ρ is the density of air and C_N and C_T are the force coefficients for respectively the normal force and tangential force, based on [23].

b. Wing pitch motion

Calculation of forces for a rotating wing is based on *flutter analysis* [24]. The expression for the normal force is

$$F_{Nr} = \pi\rho\left(\frac{3}{4} - \hat{x}_0\right)\dot{\alpha}\dot{\phi}R^2\bar{c}^2\int_0^1 \hat{c}^2(r)\hat{r}d\hat{r} \tag{5}$$

where $\hat{c} = \frac{c}{\bar{c}}$, $\bar{c}$ is the mean chord length and $\hat{r} = \frac{r}{R}$.

c. Thrust enhancing mechanisms

Mechanisms that increase the forces generated by the wing have to be taken into account. The mechanisms that are included in the analysis are *wake capture* and *delay of leading edge stall* [23]. These mechanisms are typical for flapping wing flight. The principal improvement of wake capture occurs at stroke reversal. The optimum value for the parameter ψ needs to be identified. Delay of the leading edge stall increases the forces which are generated during the wing stroke phase. To take this mechanism into account, the force component due to the stroke motion needs to be adapted. This is done by an empirical identification of the coefficient C_N.

III. Results and analysis

A. Forces generated by one wing

Hovering flight is used as a starting point and the different wing motion parameters are modified to investigate their effect on thrust and drag generation. When one wing stroke parameter is changed, the other parameters remain constant to be able to draw conclusions about one particular

parameter. From now on, only mean forces and moments are used as they are averaged over a complete flapping cycle [12].

In a first phase of this study, only one wing is modelled. Flapping frequency is set at 25 Hz. Results are in good agreement with the results of other research groups [6, 7].

B. Roll, pitch, and yaw moments generated by the wing pair

This section describes a change in the wing motion parameters of both the left and the right wing. Such a change generates a resulting moment on the nanorobot. The vehicle is considered to hover in its reference attitude when the change in wing motion parameters is applied. Roll, pitch and yaw moments are considered. The definitions of the moments with positive rotational directions are shown in Fig. 2.

1. Roll moment

Several principles are capable of generating a roll moment. The parameters that are available for modification are frequency [12], inclination angle [16] and stroke amplitude [17].

Because the wing pitch is not actively controlled in the current configuration of the Kulibrie prototype, modification of the inclination angle is not possible and generation of a roll moment can only be done through a variation of the frequency or the stroke amplitude. Because the actuation mechanism of the nanorobot is resonance based and a frequency modulation leads to a decrease in efficiency of the system, the preferred method to generate a roll moment is using differential stroke amplitude (see Fig. 5a, where the dashed lines indicate the stroke range without amplitude modulation and the shaded area indicates the stroke motion with amplitude modulation). Accurate roll control is possible with this method when applied experimentally to the prototype in the lab. Fig. 5b shows the variation of the roll moment with the stroke difference (expressed in centiNewton millimeter, or 10^{-5}Nm). Because the forces vary with the square of the stroke amplitude, the roll moment varies quadratically. Because of the small amplitude of the stroke difference, this variation looks as if it is linear in Fig. 5b.

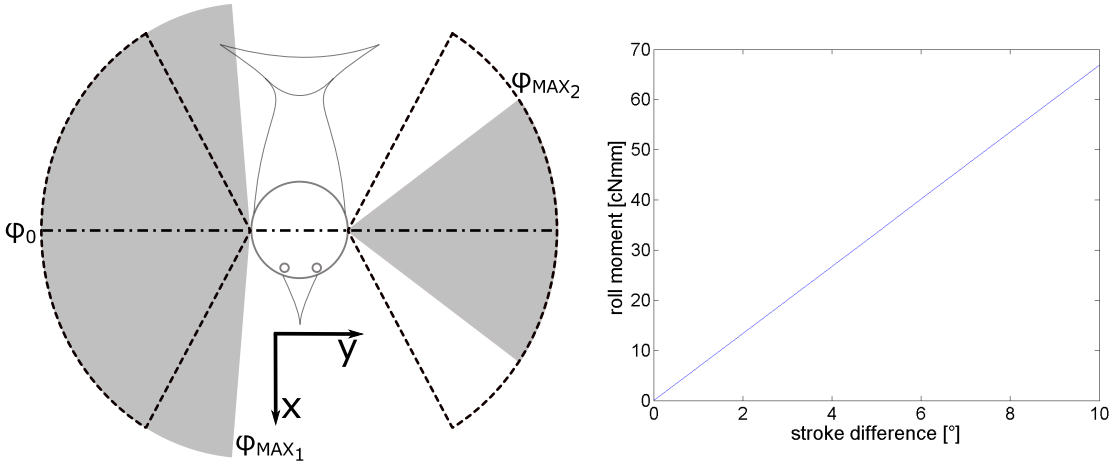

a) b)

Fig. 5 Roll moment: a) top view of nanorobot with amplitude modulation and b) moment that can be generated as a function of the stroke difference.

2. Pitch moment

a. Shift of the mean wing stroke angle

A pitching moment can be generated using a shift of the mean wing stroke angle [15, 17]. The right and left wing are changed in the same sense (see Fig. 6a). A forward shift (as shown in the figure)

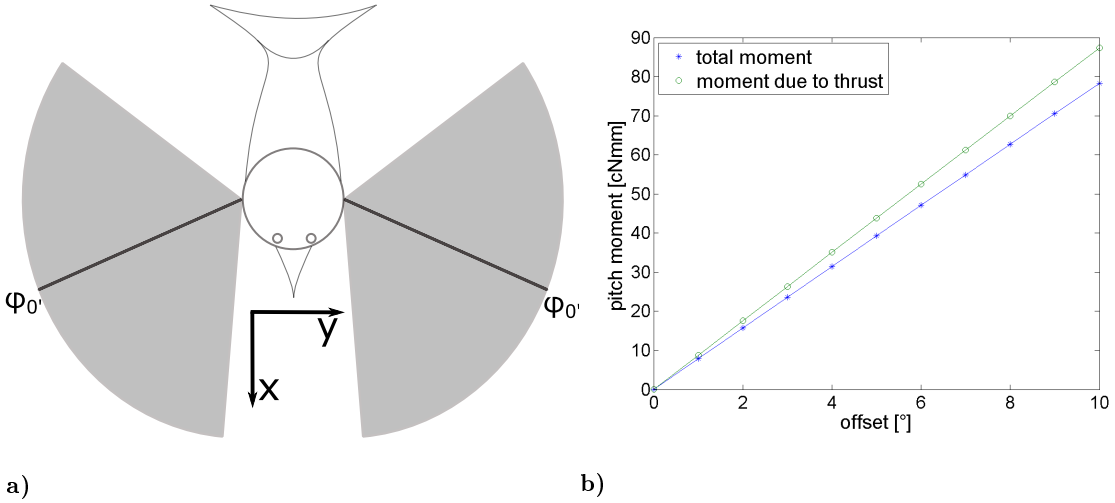

a) b)

Fig. 6 Pitch moment: a) top view of the wings with mean wing stroke angle offset and b) moment that can be generated as a function of the offset.

causes a positive moment for the nanorobot.

When the shift is done without changing the stroke amplitude, the magnitude of the mean thrust over one complete wing cycle remains unchanged. Figure 6b gives the mean moment due to the thrust as a function of the offset position. This is a sinusoidal function which is almost linear for the small offset angles shown. The offset position is expressed in degrees with respect to the reference situation and it is positive for a forward shift and negative for a backward shift. Simulations with 10° forward offset result in a mean pitch moment of 87.3 cNmm. The resulting moment due to the drag force is small compared to the moment generated by the thrust vector. The influence on the behaviour of the nanorobot is negligible.

b. Split-cycle constant period frequency modulation

Split-cycle frequency modulation [12] implies an alternation of a fast stroke and a slow stroke as shown in Fig. 7a. A fast backward stroke and slow forward stroke (as shown in the figure) generates a negative moment on the nanorobot.

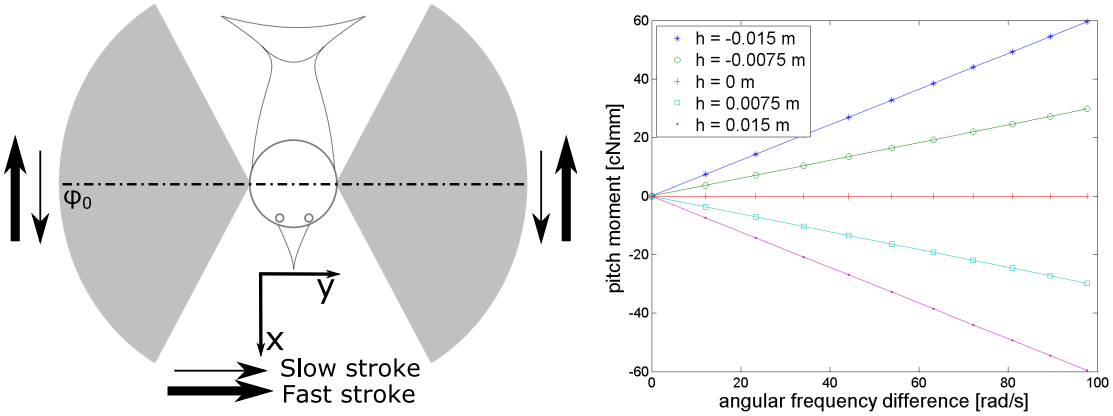

a) b)

Fig. 7 Pitch moment: a) top view of the wings with frequency modulation and b) moment that can be generated as a function of frequency difference.

The main effect of frequency modulation is that the magnitude of the drag vector increases in the fast stroke phase and decreases in the slow stroke phase. The value of the pitching moment is a function of the vertical distance h from the centre of gravity to the shoulder and of the angular frequency difference $\Delta\omega$ (with $\Delta\omega$ positive for a fast backward stroke and a slow forward stroke).

The effect is shown in Fig. 7b. Linearity is a result of the fact that the period of the wing motion is unchanged. Simulations with an angular frequency difference of 20π rad/s give a mean pitch moment generated by the drag force of -38.5 cNmm.

Side effects of the frequency modulation are a change to the magnitude of the thrust vector as well as a pitch moment due to the thrust. Simulations with the Kulibrie parameters indicate that these effects are negligible.

Comparison of pitch methods

Two aspects have to be taken into account: the ease of implementation and the numerical value obtained with the methods. The effectiveness of the first method is higher. Implementation of the first method is feasible by application of a bias to the motor voltage. Only an adequate motor control system is required, which is already available in the Kulibrie prototype. A change in the mean wing stroke angle is thus preferred to control the pitch rotation.

3. Yaw moment

a. Split-cycle constant period frequency modulation

Similar to the case of the pitching moment, split-cycle constant period frequency modulation

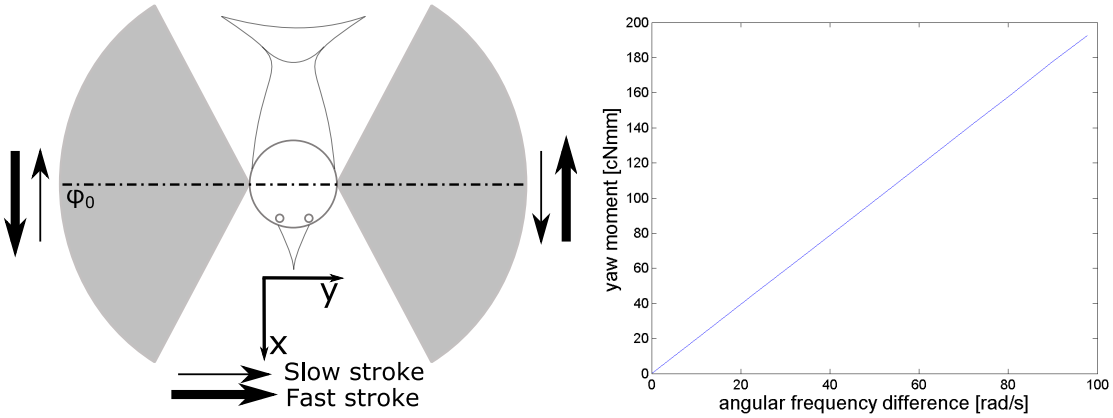

a) b)

Fig. 8 Yaw moment: a) top view of the wings with frequency modulation and b) moment that can be generated as a function of frequency difference.

[12] uses an alternation of a fast and a slow wing stroke phase but now frequency modulation is asymmetric (see Fig. 8a). A positive yaw moment is generated in the figure.

The yaw moment is generated by the drag force. The yaw moment magnitude depends on the difference in angular frequency $\Delta\omega$ between the fast stroke phase and the slow stroke phase (with $\Delta\omega$ positive when the left wing has first a fast stroke phase and then a slow stroke phase). Fig. 8b shows the mean moment as a function of $\Delta\omega$. Linearity results from the fact that the period of the wing motion is unchanged. Simulations show that no roll or pitch moment is generated by the drag force.

b. Shift of the mean wing stroke angle

Similar to the case of the pitching moment, this method uses a shift of the mean wing stroke angle [17] but now the shift of the left and right wing is in the opposite direction. A negative moment is generated by a forward shift of the right wing and a backward shift of the left wing, as shown in Fig. 9a.

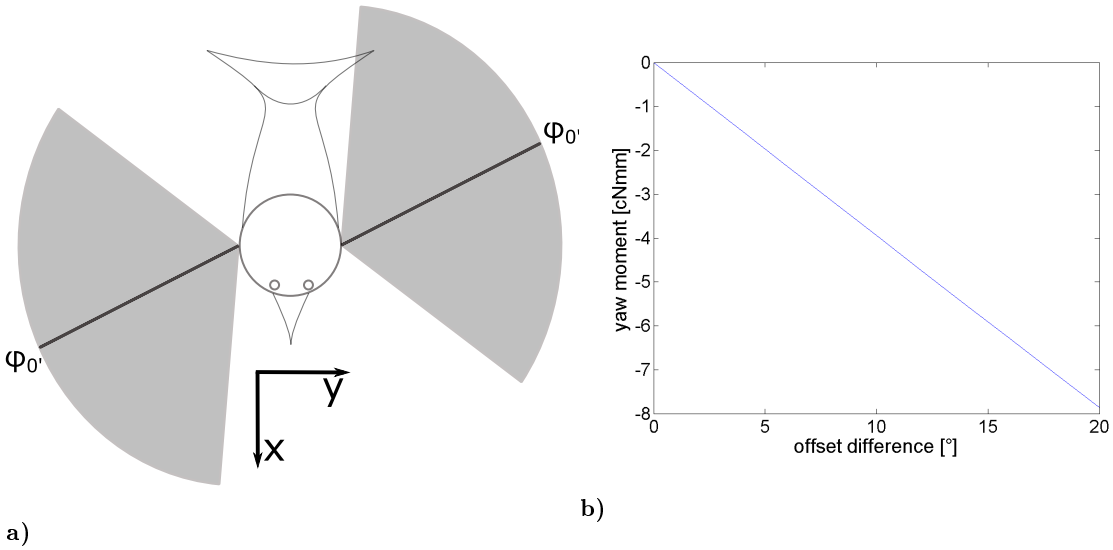

a)

b)

Fig. 9 Yaw moment: a) top view of the wings with mean wing stroke angle offset and b) moment that can be generated as a function of offset difference.

To understand the effect of the drag, different scenarios need to be considered. First, it is assumed that the shoulder of the wing is positioned exactly above the centre of gravity. In this case, the drag vector acts on a circle with radius $R \cdot \hat{r}_2$. The direction is orthogonal to the radius and

no net yaw moment is present. A second possibility is that the shoulder is placed outwards with respect to the centre of gravity with a distance e. Now, the drag vector is responsible for a small yaw moment that depends on the offset difference Δs of the mean wing stroke angle (Δs is positive for a forward shift of the right wing and a backward shift of the left wing). Fig. 9b shows the total moment as a function of Δs. This function has a sine-like pattern and it is thus close to linear for the small angles shown.

c. Shift of the mean wing stroke angle in combination with inclined stroke plane

This method is a variant to the previous concept. In this case, another geometrical configuration of the nanorobot is used. The flapping of the wings does not occur in the horizontal plane, but in a plane inclined with respect to the horizontal plane (see Fig. 10a). The definitions of thrust and drag are unchanged.

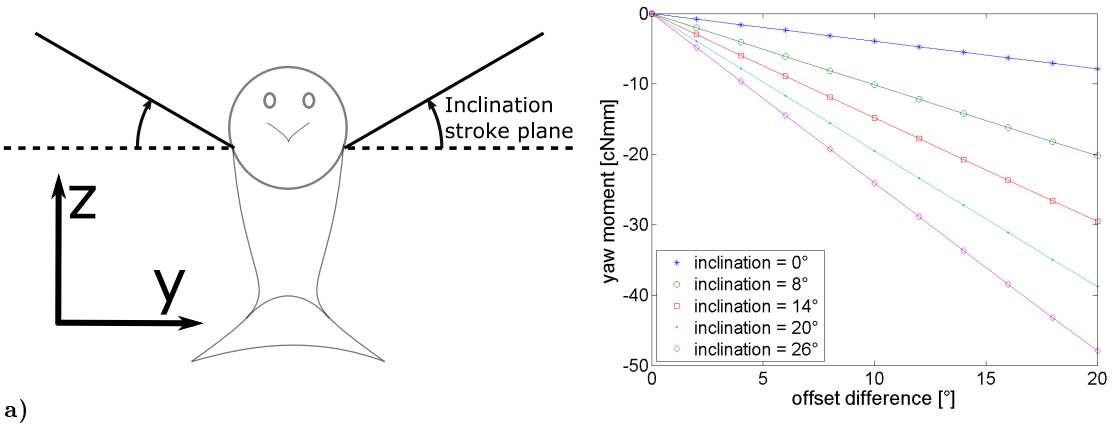

a)

b)

Fig. 10 Yaw moment: a) front view of the wings with stroke plane inclination and b) moment as a function of offset and stroke plane inclination.

The magnitude of the resulting thrust force changes parabolically with the angle of inclination. With the current parameter settings, a maximum is found for $\Delta i = 13°$. The resulting moment due to drag is a function of the angle of inclination of the flapping plane Δi and of the offset of the mean wing stroke angle Δs. Fig. 10b shows the influence of Δs on the mean moment for different values of Δi. Again, these functions have a sine-like pattern and they are close to linear for small angles.

d. Shift of the mean wing stroke angle in combination with altered inclination angle

This method is again a variant on the second concept. The difference with the second method is that the profile of the inclination angle of the wing is changed in order to change the force vectors [16]. In the simulations, this is done by setting the parameter of advanced rotation ψ to a value ψ^* once every period as shown in Fig. 11a. Fig. 11b shows the yaw moment as a function of the offset Δs and amount of advanced rotation ψ^*.

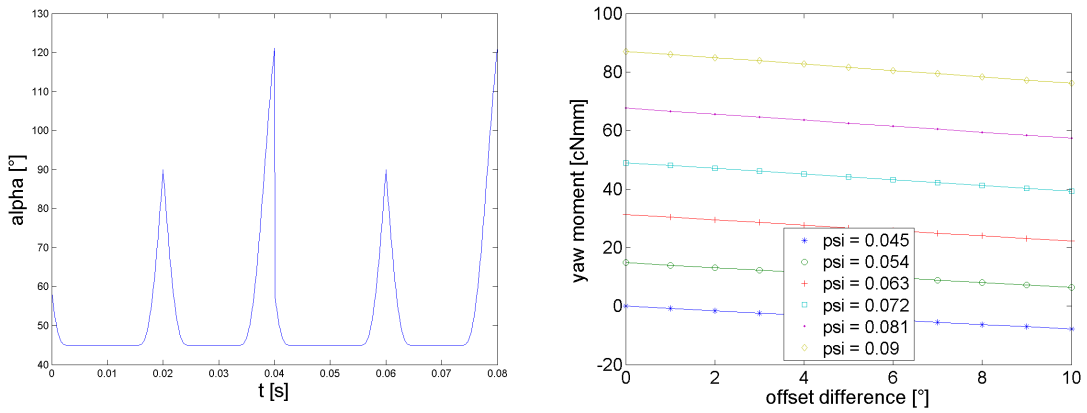

a) **b)**

Fig. 11 Yaw moment: a) asymmetric course of the inclination angle α and b) moment as a function of offset and ψ.

e. Wriggle

This method is called *wriggle steering* [18]. It uses the laws of kinematics and rotation matrices. Instead of directly rotating around the yaw axis, a sequence of rotations is done around the roll and pitch axes as shown in Fig. 12. The sequence that leads to a positive yaw rotation is a positive roll motion, a positive pitch motion, a negative roll motion and finally a negative pitch motion.

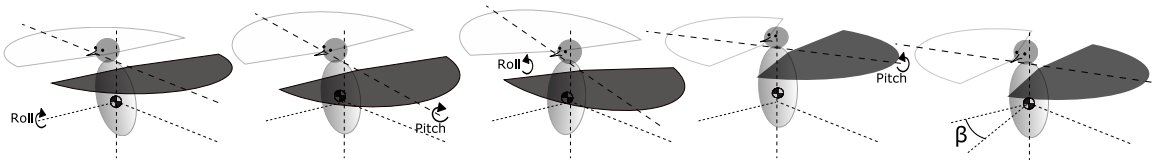

Fig. 12 Sequence of rotations leading to yaw rotation.

The order of the rotations in the sequence is important. The sequence is repeated multiple

times to get a yaw rotation that can be used for motion control. Magnitude of the rotations in the sequence have to be limited to minimize unwanted non-linearity effects. More details on the wriggle method are given by Fuller et al. [18].

Fig. 13 shows the variation of the yaw angle. The cycle-averaged yaw moment cannot be calculated for this method because the yaw moment is generated indirectly via roll and pitch moments.

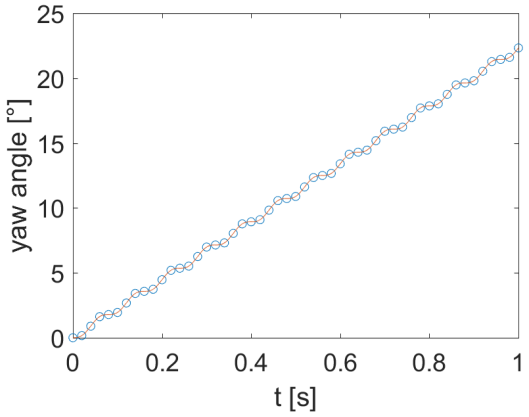

Fig. 13 The resulting change in yaw angle using *wriggle*.

Comparison of yaw methods

Again, both the ease of implementation and the effectiveness of methods need to be evaluated. As to the latter criterion, the method using split-cycle constant period frequency modulation is clearly preferred. This method is also implemented easily in the controller. However, the actuator system is assisted by the phenomenon of resonance through a properly designed elastic element. Flapping at other frequencies than resonance is disadvantageous for the efficiency of the system. For this reason also other methods have to be considered. Wriggle is in this view a good alternative because it uses roll and pitch rotations which are easier to generate with the current design.

IV. Conclusion

This paper develops a model for calculating aerodynamic forces which are generated by the flapping wings of a nano air vehicle. This model is used to conduct a sensitivity analysis on geometrical parameter changes of the nanorobot. The effect of changing motion parameters for both

wings on flight performance and steering moments is predicted. The Kulibrie nanorobot, which is currently in development at KU Leuven, is taken as a reference for the evaluation of options for the generation of steering moments.

First, to generate a roll moment, the preferred method is the application of a different stroke amplitude to both wings. Next, two methods are studied to generate a pitch moment. The method based on a change of the mean wing stroke angle is preferred because the effectiveness is higher and it is easily implemented in the current nanorobot. Finally, five concepts are studied to generate a yaw moment. Based on the numerical values, the method using split-cycle constant period frequency modulation is preferred. With a resonance supported driveline concept this method leads to a decrease in efficiency of the actuating mechanism and it is still necessary to evaluate other methods experimentally.

The proposed analysis procedure is a useful tool for an accurate assessment of different methods to change the roll, pitch and yaw angles. New methods to change these angles can be easily simulated with this tool and compared with existing methods. The results of the analysis, although not numerically exact, can be used to make design decisions on how to provide directional control and stability for a flapping wing nanorobot.

Acknowledgements

The authors gratefully acknowledge the financial support of the funding agency FWO Vlaanderen.

References

[1] Ellington, C. P., van den Berg, C., Willmott, A. P., Thomas, A. L. R., Willmott, P., and Thomas, A. L. R., "Leading edge vortices in insect flight," *Nature*, Vol. 384, 1996, pp. 626–630, doi:10.1038/384626a0.

[2] Sun, M. and Tang, J., "Unsteady aerodynamic force generation by a model fruit fly wing in flapping motion." *The Journal of experimental biology*, Vol. 205, No. 1, 2002, pp. 55–70.

[3] Zhang, Y. L. and Sun, M., "Dynamic flight stability of a hoveringmodel insect: lateral motion," *Acta Mechanica Sinica/Lixue Xuebao*, Vol. 26, No. 4, 2010, pp. 509–520, doi:10.1007/s10409-009-0303-1.

[4] Taylor, G. K. and Thomas, A. L. R., "Dynamic flight stability in the desert locust Schistocerca gregaria." *The Journal of experimental biology*, Vol. 206, No. Pt 16, 2003, pp. 2803–2829, doi:10.1242/jeb.00501.

[5] Sun, M. and Tang, J., "Lift and power requirements of hovering flight in Drosophila virilis." *The Journal of experimental biology*, Vol. 205, No. 16, 2002, pp. 2413–2427.

[6] Wu, J. H., "Unsteady aerodynamic forces of a flapping wing," *Journal of Experimental Biology*, Vol. 207, No. 7, 2004, pp. 1137–1150, doi:10.1242/jeb.00868.

[7] Wu, J. H., Sun, M., and Zhou, Z. W., "Control of flight forces and moments by flapping wings of model bumblebee," *Applied Mathematics and Mechanics (English Edition)*, Vol. 29, No. 3, 2008, pp. 333–350, doi:10.1007/s10483-008-0305-x.

[8] Ramamurti, R. and Sandberg, W. C., "A three-dimensional computational study of the aerodynamic mechanisms of insect flight." *The Journal of experimental biology*, Vol. 205, No. 10, 2002, pp. 1507–1518.

[9] Xiong, Y. and Sun, M., "Dynamic flight stability of a bumblebee in forward flight," *Acta Mechanica Sinica/Lixue Xuebao*, Vol. 24, No. 1, 2008, pp. 25–36, doi:10.1007/s10409-007-0121-2.

[10] Berman, G. J. and Wang, Z. J., "Energy-minimizing kinematics in hovering insect flight," *Journal of Fluid Mechanics*, Vol. 582, 2007, pp. 153, doi:10.1017/S0022112007006209.

[11] Sane, S. P. and Dickinson, M. H., "The aerodynamic effects of wing rotation and a revised quasi-steady model of flapping flight." *The Journal of experimental biology*, Vol. 205, No. 8, 2002, pp. 1087–1096.

[12] Doman, D. B., Oppenheimer, M. W., and Sigthorsson, D., "Dynamics and control of a minimally actuated biomimetic vehicle: Part i-aerodynamic model," *Proceedings of the AIAA Guidance, Navigation, and Control Conference*, , No. 6160, 2009, pp. 1–25, doi:10.2514/6.2009-6160.

[13] Karasek, M. and Preumont, A., "Flapping Flight Stability in Hover: A Comparison of Various Aerodynamic Models," *International Journal of Micro Air Vehicles*, Vol. 4, No. 3, 2012, pp. 203–226, doi:10.1260/1756-8293.4.3.203.

[14] Whitney, J. P. and Wood, R. J., "Aeromechanics of passive rotation in flapping flight," *Journal of Fluid Mechanics*, Vol. 660, 2010, pp. 197–220, doi:10.1017/S002211201000265X.

[15] Anderson, M. L. and Cobb, R. G., "Toward Flapping Wing Control of Micro Air Vehicles," *Journal of Guidance, Control, and Dynamics*, Vol. 35, No. 1, 2012, pp. 296–308, doi:10.2514/1.51170.

[16] Keennon, M., Klingebiel, K., Won, H., and Andriukov, A., "Tailless Flapping Wing Propulsion and Control Development," *Proc. of 50th AIAA Aerospace Science Meeting, Nashville, TN, January*, , No. 588, 2012, pp. 1–24.

[17] Ma, K. Y., Chirarattananon, P., Fuller, S. B., and Wood, R. J., "Controlled Flight of a Biologically Inspired, Insect-scale robot," *Science*, Vol. 340, May 2013, pp. 603–608, doi:10.1126/science.1231806.

[18] Fuller, S. B., Whitney, J. P., and Wood, R. J., "Rotating the heading angle of underactuated flapping-wing flyers by wriggle-steering," *International Conference on Intelligent Robots and Systems*, 2015, pp. 1292–1299, doi:10.1109/IROS.2015.7353535.

[19] Karasek, M., Hua, A., Nan, Y., Lalami, M., and Preumont, A., "Pitch and Roll Control Mechanism for a Hovering Flapping Wing MAV," *Int. J. Micro Air Veh.*, Vol. 6, No. 4, 2014, pp. 253–264, doi:10.1260/1756-8293.6.4.253.

[20] Doman, D. B., Oppenheimer, M. W., and Sigthorsson, D., "Dynamics and control of a minimally actuated biomimetic vehicle: Part ii-control," *Proceedings of the AIAA Guidance, Navigation, and Control Conference*, , No. 6161, 2009, pp. 1–23, doi:10.2514/6.2009-6161.

[21] Leys, F., Reynaerts, D., and Vandepitte, D., "Outperforming hummingbirds' load-lifting capability with a lightweight hummingbird-like flapping-wing mechanism." *Biology open*, Vol. 213, No. 5, 2016, pp. 725–734, doi:10.1242/bio.014357.

[22] Anderson, J. D., "Fundamentals of Aerodynamics," 2011, pp. 277–350.

[23] Dickinson, M. H., Lehmann, F. O., and Sane, S. P., "Wing rotation and the aerodynamic basis of insect flight." *Science (New York, N.Y.)*, Vol. 284, No. 5422, 1999, pp. 1954–1960, doi:10.1126/science.284.5422.1954.

[24] Fung, Y., "An Introduction to the Theory of Aeroelasticity." 1969.